Available online at www.sciencedirect.com
SCIENCE DIRECT
Acta Materialia 54 (2006) 1559–1569
Acta MATERIALIA
www.actamat-journals.com

Wettability of polycrystalline rutile TiO_2 by molten Al in different atmospheres

Ping Shen [a,b,*], Hidetoshi Fujii [a], Kiyoshi Nogi [a]

[a] Joining and Welding Research Institute, Osaka University, 11-1 Mihogaoka Ibaraki, Osaka 567-0047, Japan
[b] Key Laboratory of Automobile Materials, Department of Materials Science and Engineering, Jilin University, 5988 Renmin Street, Changchun 130025, PR China

Received 18 August 2005; received in revised form 8 November 2005; accepted 15 November 2005
Available online 19 January 2006

Abstract

Sessile drop experiments were performed to study the wettability of polycrystalline rutile TiO_2 by molten aluminum in purified Ar, Ar–3% H_2 and vacuum over a wide temperature range. The effects of atmosphere, temperature, time and testing method on the contact angles were thoroughly investigated and the resulting interfacial microstructures were examined. The atmosphere- and temperature-dependent reduction in the TiO_2 substrates was manifested by (i) distinct color change of the crystals before and after annealing and (ii) color variation in the crystals produced in different atmospheres and at different temperatures. The wetting results were explained on the basis of TiO_2 surface chemistry and competition reactions between Al surface oxidation and deoxidation. With regard to the contact angles, which are generally smaller than 90° in well-controlled Ar and vacuum, the Al–TiO_2 system is of a partial wetting nature. However, this system can easily be non-wetting due to a considerable increase in the oxygen partial pressure as a result of TiO_2 reduction, particularly in a hydrogen-containing atmosphere.

Keywords: Wetting; Ceramic; Reaction; Interface; Microstructure

1. Introduction

Al–TiO_2 is an intriguing system since it can be used to produce alumina-reinforced titanium aluminide alloys (3A) with interpenetrating network microstructures, which exhibit high strength, high fracture toughness, low specific structural weight and good resistance to corrosion, wear and creep [1,2]. This 3A material has been successfully produced by many researchers using various synthesis techniques, such as reactive squeeze casting [2–5], pressure-aided reactive infiltration [2,6,7], reactive sintering [1,8] and reactive ball milling [9,10]. For instance, researchers [2–5] have produced α-Al_2O_3-reinforced $TiAl_3$ composites by squeeze casting of molten aluminum into whisker or particulate TiO_2 or $TiO_2 + Al_2O_3$ preforms. Gheorghe and Rack [6,7] fabricated composites of fully reacted and partially reacted alumina with Ti–Al ($TiAl_3$ and $TiAl_2$) intermetallic compounds by pressure-aided reactive infiltration of molten Al into TiO_2 whiskers. The reactions in this system with different Al/TiO_2 ratios can be expressed by the following overall equation:

$$Al + TiO_2 \rightarrow Al_2O_3 + Ti_xAl_y \quad (1)$$

The type of titanium aluminide formed, e.g., $TiAl_3$, $TiAl_2$, TiAl or Ti_3Al, depends on the ratio of Al to TiO_2 in the reactants, and the type of alumina, such as δ-, η-, γ- and α-phases, depends on the temperature.

A critical factor that governs the infiltration process is the physicochemical properties at the solid–liquid interface such as the work of immersion, W_i, which is given by

* Corresponding author. Tel./fax: +86 431 5094699/81 6 6879 8663.
E-mail addresses: shp1972@163.com, shp1972@126.com (P. Shen).

1359-6454/$30.00
doi:10.1016/j.actamat.2005.11.024

$$W_i = \sigma_{sl} - \sigma_{sv} \quad (2)$$

where σ_{sl} and σ_{sv} are the solid–liquid and solid–vapor interface free energies, respectively. If $\sigma_{sv} > \sigma_{sl}$, the liquid metal wets and spontaneously penetrates into the solid, whereas in the opposite case, work is required to make the solid–liquid interface. Thus, infiltration of a liquid into a porous preform in the non-wetting case will require a minimum external pressure, P_0, which can be written as [11]

$$P_0 = S_i(\sigma_{sl} - \sigma_{sv}) \quad (3)$$

where S_i is the surface area of the interface per unit volume of the metal matrix. P_0 can be related to the contact angle θ at the solid–liquid interface using Young's equation

$$\sigma_{sv} = \sigma_{sl} + \sigma_{lv}\cos\theta \quad (4)$$

where σ_{lv} is the liquid–vapor interface free energy. Therefore, Eq. (3) can be rewritten as

$$P_0 = -S_i\sigma_{lv}\cos\theta \quad (5)$$

which establishes a simple relationship between the contact angle and the threshold pressure for infiltration.

The wettability of TiO_2 by molten Al has been recently investigated by Sobczak et al. [12] and Avraham and Kaplan [13]. The former study focused on the effects of temperature and testing procedure on the wettability and it was found that by using a common contact heating method (i.e., a small Al rod was pre-placed on a TiO_2 substrate and then the couple were heated together to the testing temperature) TiO_2 was wetted by the oxidized molten Al at $T > 1210$ K in vacuum. The removal of the oxide film from the Al drop surface by means of a capillary purification procedure makes the system wettable at 1173 K. Nevertheless, the time variation of the contact angle, i.e., the wetting kinetics, at a constant temperature was not presented. The study of Avraham and Kaplan focused on the wetting kinetics and it was argued that the spreading of an Al drop on the TiO_2 surface was governed by the reduction reaction at the solid–liquid interface. The contact angle was found to be very large at 973 K (~150°) but tended to decrease with increasing temperature. At 1273 K, the contact angle changed from ~125° to a steady value of ~85° after 120 min [13]. The reaction in sessile drop samples was found remarkable only at high temperatures, e.g., 1373 K [12]. Accordingly, much higher temperatures were required for the successful synthesis of Ti–Al/Al_2O_3 composites from Al–TiO_2 reactants. This result seems to be in contradiction to the behaviors observed in the aforementioned synthesis processes, where a strong reaction was generally observed at $T \geqslant 1073$ K, resulting in reaction products at the interface [1–7].

In this study, we carried out a systematic investigation of the wettability of rutile TiO_2 by molten Al. The effects of atmosphere, temperature, time and testing method were examined. The wetting results were explained on the basis of TiO_2 surface chemistry and competition reactions between Al surface oxidation and deoxidation. In addition, interfacial reactions and the resulting microstructures were analyzed. Reasons for the discrepancy in the microstructures observed in the sessile drop samples and in the reaction synthesized samples were also addressed.

2. Experimental

The substrates used in this study were high-purity (99.9 wt.%) polycrystalline rutile TiO_2 tablets with dimensions of 20 mm (diameter) × 5 mm (Kojundo Chemical Co. Ltd, Saitama, Japan). Incorporated impurities included 0.001 wt.% Ca, 0.001 wt.% Cr and 0.002 wt.% Fe. The surfaces of the TiO_2 were mechanically ground on diamond discs and carefully polished using diamond pastes down to 0.25 μm to obtain an average surface roughness (R_a) of less than 100 nm, which was measured using a Dektak 3 surface profilometer (Veeco Instruments Inc., NY) over a scanning distance of 2 mm at a speed of 80 μm/s. High-purity (99.99 wt.%) Al samples weighing about 0.12–0.14 g were in the form of wire segments with a diameter of 3 mm. To remove surface oxide film, the Al samples were first cleaned in a 20 wt.% NaOH distilled water solution for 15 min using a magnetic stirring machine at ~313 K, immediately rinsed with water and ethanol and then ultrasonically cleaned in acetone. The TiO_2 substrates were also ultrasonically cleaned before being placed in the chamber.

The experimental apparatus, as illustrated schematically in Fig. 1, consisted of a two-window stainless steel chamber, with a tantalum cylindrical heater shielded by five-layer concentric Mo reflectors, an evacuating system with a rotary pump and a turbomolecular pump, a dropping device, a temperature program controller with a W5-type (W–5% Ra/W–26% Rh) thermocouple, a 10 mW He–Ne laser (Melles Griot, Carlsbad, CA) for illumination, a band-pass filter and a high-resolution digital camera with 2000 × 1312 pixels. The band-pass filter can cut all wavelengths except for the laser beam (wavelength = 632.8 nm); therefore, high-definition drop profiles can be obtained.

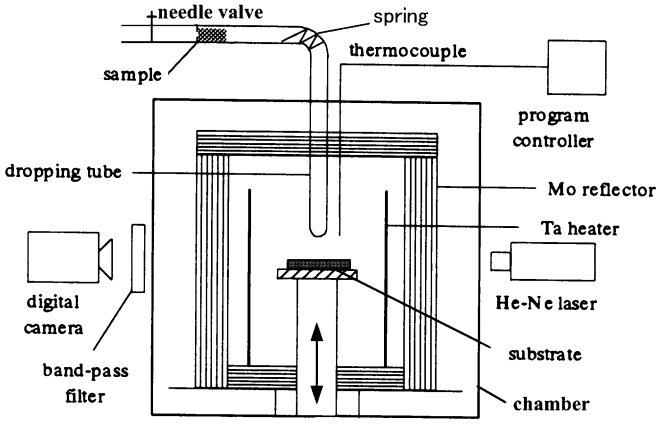

Fig. 1. Schematic of the experimental apparatus (side view). The Al sample was first placed outside the chamber and it could be dropped into the chamber through the dropping tube at any desired testing temperature. The alumina dropping tubes have two kinds of holes with diameters of 1 and 4 mm, respectively, at their ends.

The wetting experiments were performed mainly using an improved sessile drop method, in which molten Al was deposited out of an alumina tube (99.6 wt.%) with a small hole (diameter = 1 mm) at the bottom and then dropped onto the TiO_2 surface at the desired testing temperatures. This method offers the advantage of further removal of the Al surface oxide film by mechanical extrusion. Two dropping modes, i.e., an impingement mode (I-mode) and a non-impingement mode (NI-mode) [14], were adopted. In the I-mode, the dropping distance between the bottom of the alumina tube and the surface of the substrate was controlled to be slightly larger than the drop height, so that the aluminum drop could directly form after the liquid was extruded. In the NI-mode, however, the dropping distance was controlled to be slightly less than the drop height and thereby the extruded liquid could contact both the substrate and the bottom of the tube. The substrate was then slightly lowered for the drop to break away from the tube. This process generally finished within 10–15 s. In addition, for comparison purposes, a limited number of experiments were conducted using a modified conventional sessile drop method, in which the Al sample was directly dropped from the alumina tube with a large hole (diameter = 4 mm) at its bottom, thus without any mechanical removal of the oxide film.

After ultrasonic cleaning, the TiO_2 substrate was placed horizontally in the chamber while the Al segment was placed in a glass tube with a spring connector on the top of the dropping device outside the chamber (see Fig. 1). The chamber was first evacuated to a pressure of $\sim 4 \times 10^{-4}$ Pa at room temperature and then heated to the desired testing temperature in vacuum at a rate of 20 °C/min. The wetting experiments were performed in three different atmospheres: (1) a flowing (1 L/min) Ar atmosphere, (2) a flowing (1 L/min) Ar–3% H_2 atmosphere, and (3) a vacuum. In cases (1) and (2), the gases were purified through a delicate gas-purification system to reduce water and oxygen levels before the gases were introduced into the chamber. For example, the Ar gas (99.999% purity) was first purified by flowing it through tubes filled with zeolite and $Mn + MnO_2$ materials, and then through Cu tubes cooled by dry ice in ethanol to remove water. The gas then passed through a magnesium furnace at temperatures controlled to 823 ± 2 K to reduce the oxygen and water and again through the dry ice-cooled Cu tubes. The Ar–3% H_2 gas was purified by platinum asbestos and magnesium perchlorate. The oxygen partial pressures, as measured by a ZrO_2–11 mol% CaO solid electrolyte oxygen sensor at 1073 K, were of the order of 10^{-15} Pa in purified Ar and 10^{-18} Pa in purified Ar–3% H_2. The atmospheric pressure inside the chamber was controlled at about 0.11–0.12 MPa. After the temperature and the atmosphere had stabilized, the Al segment was inserted into the bottom of the alumina tube. Molten Al was then forced out through a small hole (diameter = 1 mm) at the bottom of the tube and dropped onto the TiO_2 surface after a time ~50 s when a gas pressure difference between inside of the tube and inside of the chamber was created by the gas outflow.

For the experiments in case (3) (i.e., vacuum), two testing methods were adopted: (1) the Al wire segment (diameter = 3 mm) was directly dropped through a 4 mm diameter hole at the bottom of the alumina tube without any mechanical removal of the oxide film, and (2) the Al sample was first melted in the bottom of the alumina tube and then dropped through a 1 mm diameter hole using a trace of the purified Ar–3% H_2 gas that leaked from a needle valve (Fig. 1).

As soon as the Al drop was formed on the TiO_2 substrate, a photograph was taken and defined as the drop profile at zero time. Subsequent photographs were taken as a function of time. The photographs were analyzed using an axisymmetric drop shape analysis program, by which the contact angle, surface tension and density could be simultaneously calculated. This program offers a high degree of accuracy for calculation of the contact angle (error $\leqslant \pm 1°$) and eliminates operator's subjectivity.

After the wetting experiments, selected samples were vertically sectioned to prepare metallographic specimens. Interfacial microstructures were examined using a laser microscope (Keyence, VK-8550, Osaka, Japan) and an environmental scanning electron microscope (ESEM-2700, Nikon Co., Kanagawa, Japan) with energy dispersive X-ray microanalysis (EDAX) capability.

3. Results

3.1. Sample appearance after wetting experiments

Fig. 2 shows some representative sessile drop samples after the wetting experiments in vacuum, Ar and Ar–3%

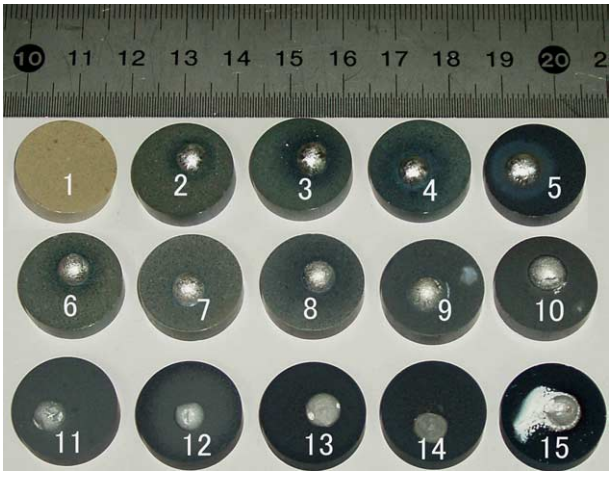

Fig. 2. Appearance of some representative sessile drop samples after the wetting experiments in vacuum (2–5), Ar (6–10) and Ar–3% H_2 (11–15) together with an original TiO_2 substrate (1) as a reference. (Experimental conditions: 2, 6 and 11: 1173 K, 1 h; 3, 7 and 12: 1273 K, 1 h; 4, 8 and 13: 1373 K, 1 h; 5: 1473 K, 2 h; 9 and 14: 1473 K, 1 h; and 10 and 15: 1573 K, 1 h. All the experiments were performed using the improved sessile drop method.)

H_2 at various temperatures together with an original TiO_2 substrate as a reference. Clearly, the color of the substrates changes from the original light yellow (before the experiment) to dark gray or black (after the experiment), and the darkness enhances with an increase in temperature, which is more marked in the samples tested in the Ar–3% H_2 atmosphere. Another distinct feature is the difference in the shape and color of the Al drops after the experiments in the three atmospheres. In vacuum and in Ar, the Al samples are basically in a spherical shape with shiny metallic surfaces, whereas in Ar–3% H_2, the Al samples are distorted and no metallic luster appears on their surfaces.

3.2. Contact angle phenomena

3.2.1. Ar atmosphere

First, we investigated the effect of the dropping modes, i.e., I-mode and NI-mode, on the contact angles obtained. Fig. 3 shows the variation in the contact angles with time at 1273 and 1373 K with these two dropping modes. As can be seen: (1) the initial contact angles obtained for the I-mode are considerably smaller than those for the NI-mode, and the former do not show a remarkable decrease with time while the latter do; (2) the contact angles obtained for the I-mode seem to be weakly dependent on the temperature, while for the NI-mode, the influence of temperature is significant; and (3) despite the initial contact angles obtained for the NI-mode at 1373 K being larger, they decrease to values closer to those for the I-mode after a certain time. At 1273 K, however, the contact angles obtained for the NI-mode are always larger during the entire wetting period.

The much larger contact angles produced by the NI-mode are most likely due to Al surface reoxidation when the substrate was slightly lowered for the extruded molten Al to detach from the alumina tube, even though this process finished in a short time (10–15 s). The influence of the dropping mode or the effect of Al surface reoxidation is therefore significant. In order to reduce the effect of Al surface reoxidation, the I-mode was employed in subsequent experiments, except for a specific requirement.

Fig. 4 shows the contact angles at various temperatures as a function of time. The contact angles seem to be only mildly dependent on the temperature. The initial contact angles, as clearly indicated in the small graph using a logarithmic time scale, however, are more temperature dependent, which increase with increasing temperature. Repeated experiments show that the initial contact angles have some extent of scatter (up to ±4°), but this distinctive temperature-dependent behavior generally recurred. For the final contact angles, the scatter is decreased, particularly for wetting at high temperatures. However, a marked continuous decrease in the contact angle with time appears only at 1573 K, implying that a strong reaction between the molten Al and the TiO_2 substrate occurs only at high temperatures.

It is worth noting that the contact angles at $T = 1173$–1273 K are always smaller than 90°. At $T > 1273$ K, although the initial contact angles are larger than 90°, they decrease to less than 90° in a relatively short time (~300 s). In this sense, it could be regarded that the Al–TiO_2 system in a well-controlled Ar atmosphere is partial wetting or at least it is easy to realize partial wetting.

3.2.2. Ar–3% H_2 atmosphere

Fig. 5 shows the contact angles at various temperatures as a function of time. In comparison with Fig. 4, the contact angles obtained in this atmosphere are larger, even though the oxygen partial pressure in the inlet gas is smaller. With an increase in temperature, the initial contact angles exhibit similar behavior as those in Ar, i.e., they generally increase with the temperature. However, the dynamic contact angles show a quite different behavior. In Ar, the contact angle decreases with time, particularly at a higher temperature, and thus the final contact angle decreases

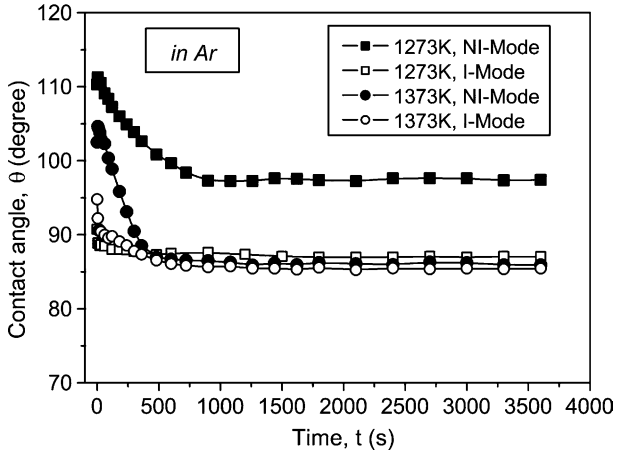

Fig. 3. Variation in the contact angles with time at 1273 and 1373 K for molten Al dropped by the NI-mode and the I-mode in the purified Ar atmosphere.

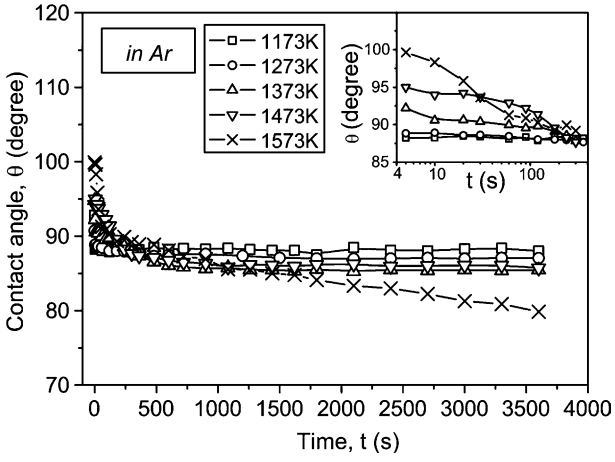

Fig. 4. Variation in the contact angles with time at various temperatures in the purified Ar atmosphere. The smaller graph shows the initial contact angles before 400 s.

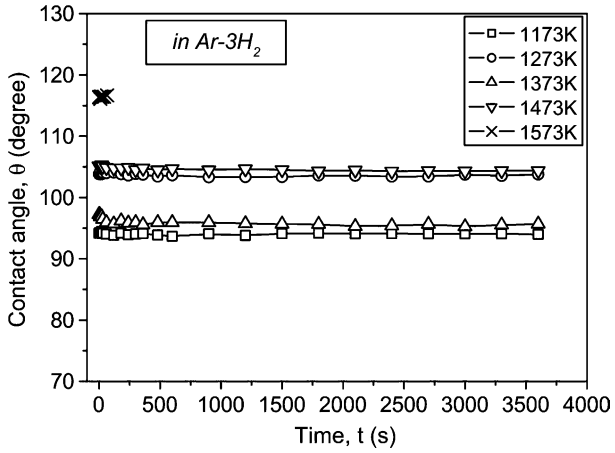

Fig. 5. Variation in the contact angles with time at various temperatures in the purified Ar–3% H_2 atmosphere. The contact angles at 1273 K were produced using the NI-mode.

with the temperature increase. But there is not such an obvious decrease in Ar–3% H_2.

Another distinct phenomenon in this atmosphere is that, at 1573 K, a smog-like reaction product was produced almost immediately after the molten Al drop was formed. Fig. 6 shows some photographs of this phenomenon. The reaction product deposited on and around the Al drop (see also no. 15 in Fig. 2) as well as on the alumina dropping tube. Energy dispersive spectroscopy (EDS) analysis (Fig. 7) indicates that the deposited white powders are fine alumina. The surface of the Al drop was completely oxidized (Fig. 7(c)). Associated with the gray color of the Al drops examined in this atmosphere (Fig. 2), it is reasonable for us to speculate that the real oxygen partial pressure, p_O, around the Al drop is much higher in Ar–3% H_2 than in Ar. More detailed explanations are presented in Section 4.

3.2.3. Vacuum

Fig. 8 shows the variation in the contact angle with temperature (during continuous heating to 1373 K at a rate of 10 K/min) and time (during dwell at 1373 K) for the Al sample dropped from a 4 mm diameter hole (without any mechanical extrusion) at 973 K (since it took at least 10 s for the Al sample to completely melt, Al was actually dropped in the solid state by this method). The initial contact angle is quite large ($\theta_{in} = 145°$) due to the Al surface being covered by its oxide film. This result is similar to that observed by Avraham and Kaplan ($\theta_{in} = 150°$) [13]. With an increase in temperature, a notable decrease in the contact angle was observed at 1004 K and 1098 K, which is thought to be a result of the partial disruption of the oxide film possibly due to the thermal expansion mismatch between the molten Al and its surface oxide film during heating. With a further increase in temperature, however, the contact angle no longer shows an appreciable decrease, and during the dwell period, only a small progressive decrease was observed.

Fig. 9 shows the variation in the contact angles with time for Al dropped in a liquid state by extruding through a 1 mm diameter hole (with mechanical extrusion) at various temperatures. The contact angles obtained are generally smaller than 90°, indicating that Al–TiO_2 is an essentially partial wetting system. As compared with Fig. 4, the contact angles obtained in vacuum are smaller than those in Ar. Two common features in Ar and in vacuum are that the initial contact angles increase with increasing temperature and a marked continuous decrease in the contact angle with time appears only at high temperatures, which are 1573 K in Ar and 1473 K in vacuum.

Fig. 10 compares the time variation of the contact angle and normalized drop base diameter for Al directly dropped at 1473 K in vacuum with two different methods (with and without mechanical extrusion). It is obvious that with mechanical extrusion, the contact angles during the early wetting stage are much smaller since the initial oxide film covering the Al surface was disrupted or removed. However, after a long dwell time (2 h), the final apparent contact angles are closer. The contact angles in both cases are advancing ones since the drop base diameter is always increasing. The relative volume loss of the Al drops due to their evaporation and reaction with the TiO_2 substrates was estimated to be ~4% for the Al dropped without extrusion and ~12% for it dropped with extrusion after a 2 h run at 1473 K in a vacuum of $\sim 5 \times 10^{-4}$ Pa.

3.3. Interfacial microstructures

Laser microscopy and ESEM examinations show that for the experiments performed in Ar–3% H_2, no substantial reaction products, except for an aluminum oxide, could be detected at the Al–TiO_2 interface. For the samples tested in Ar and in vacuum, reaction products were observed at the interfaces. The development of the reaction layer mainly depends on temperature, although time, atmosphere (Ar or vacuum) and testing method also play an important role.

Fig. 11 shows the interfacial microstructures around the triple junction in the sample tested at 1373 K for 1 h in Ar. Reaction products are visible. The EDS results indicate

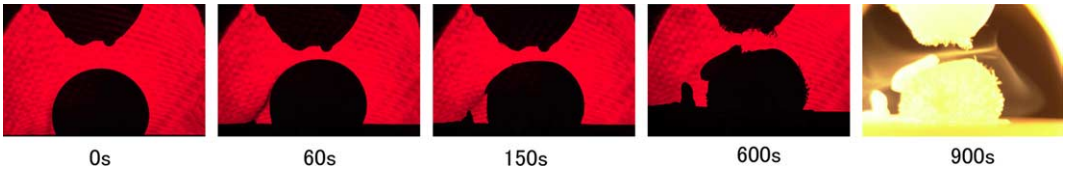

Fig. 6. Representative photographs showing the formation of a smog-like reaction product on and around the Al drop as well as on the alumina dropping tube at 1573 K in Ar-3% H_2 (at 900 s, the band-pass filter was removed to clearly show the smog).

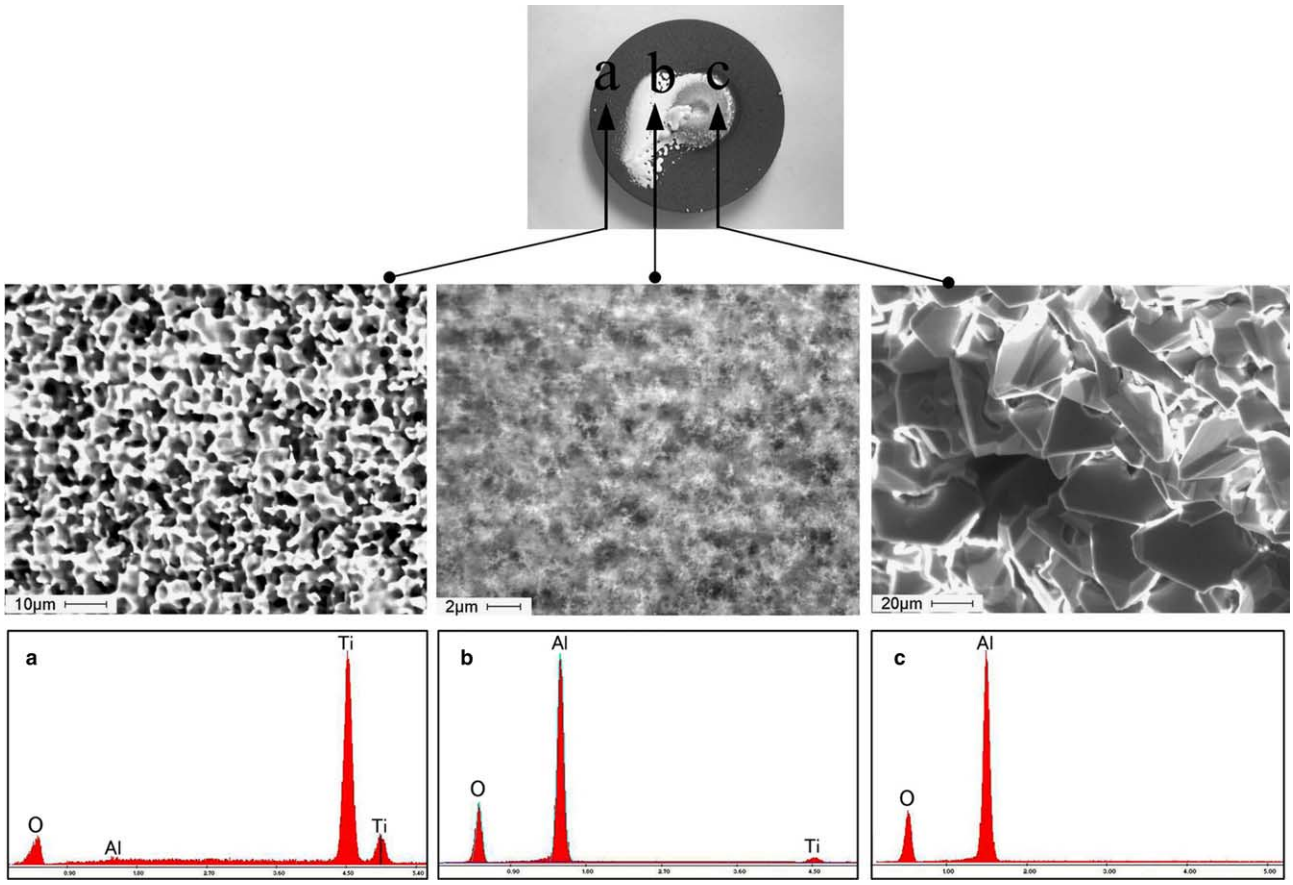

Fig. 7. ESEM micrographs showing the microstructures at positions "a", "b" and "c" of the Al–TiO_2 sample tested at 1573 K in Ar–3% H_2, and the corresponding X-ray EDS determining their compositions. The white powders formed on and around the Al drop are alumina and the surface of the Al drop is covered by its oxide film.

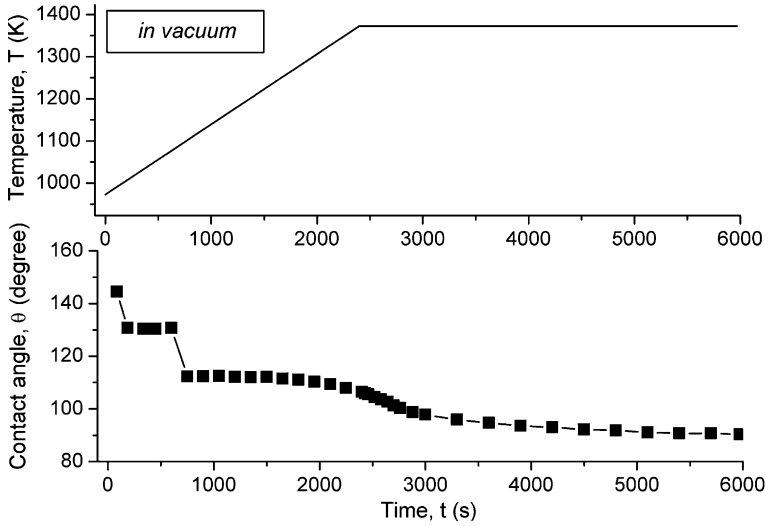

Fig. 8. Variation in the contact angle with temperature (during heating to 1373 K at a rate of 10 K/min) and time (during dwell at 1373 K) for the Al sample dropped from a 4 mm diameter hole at the bottom of the alumina tube at 973 K in vacuum (i.e., without any mechanical extrusion to remove the Al surface oxide film).

that particle-like crystals, discontinuously distributed at the interface, are primarily the alumina phase with a small amount of Ti incorporated. Beneath the interface, a heterogeneous reaction layer was formed due to Al infiltration and reaction with the bulk TiO_2 crystal, producing alumina-rich areas (dark parts such as position "b") and Ti–Al–O combined phase areas (light gray parts such as position "a").

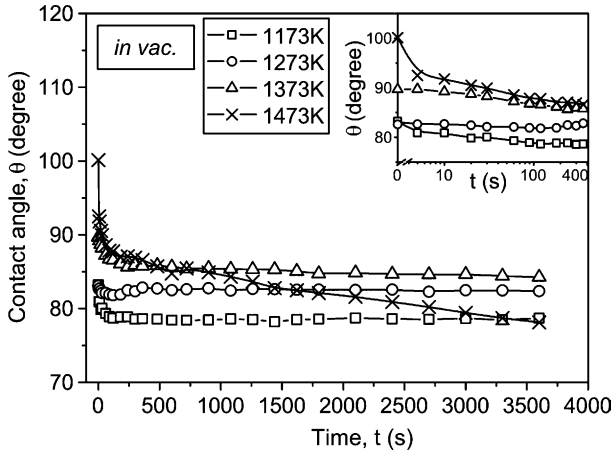

Fig. 9. Variation in the contact angles with time at various temperatures for Al dropped through a 1 mm diameter hole (i.e., with mechanical extrusion) in vacuum. The small graph shows the initial contact angles before 400 s.

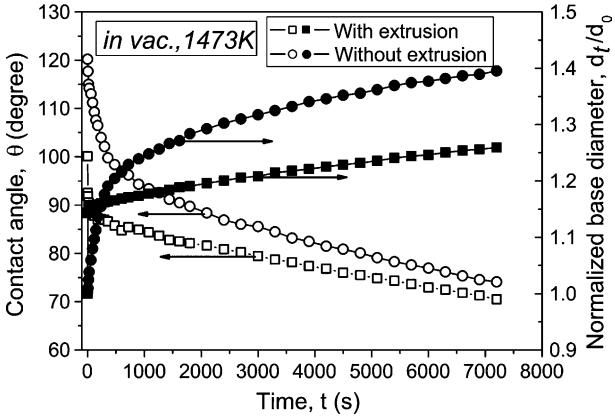

Fig. 10. Comparison of the variations in the contact angle and normalized drop base diameter with time for Al dropped at 1473 K in vacuum with and without mechanical extrusion.

Fig. 12 shows laser microscopy images of the interfacial microstructures of the samples tested at 1473 K for 2 h in vacuum for Al dropped without and with mechanical extrusion. The reaction regions beneath the Al drops in both samples are discontinuous; however, the total area of the reaction regions and the maximum thickness of the reaction layer in the latter are larger than those in the former.

Fig. 13 shows the microstructures at the interface around the triple junction in the sample tested at 1573 K for 1 h in Ar. A much thicker and continuous reaction layer was formed beneath the Al drop, indicating that the reaction between Al and TiO_2 is extensive at this temperature. The EDS analysis demonstrates that the reaction products consist mainly of $(TiAl)_xO_y$ and $(TiAl_2)_xO_y$ phases (such as in white area "2" of the central figure), which might be the intermediate products, and the alumina-rich phases with a certain amount of Ti incorporated (such as in dark area "3" of the central figure). Other Ti–Al–O combined phases like $(Ti_{27}Al_{73})_xO_y$ were also identified in the alumina-rich area. In addition, the reduced Ti was found to accumulate at the interface and form Ti–Al intermetallic compounds. The diffusion of the reduced Ti to the interface and the accumulation at the interface, particularly in regions of the triple junction, may promote wetting since Ti is usually a strong wetting-promoting element for many metal–ceramic systems [15].

4. Discussion

4.1. Reduction of the TiO_2 substrate in different atmospheres

It is well known that stoichiometric rutile TiO_2 single crystals can be reduced by annealing under vacuum conditions, producing reduced TiO_{2-x} phases with various types of point defects such as doubly charged oxygen vacancies, Ti^{3+} and Ti^{4+} interstitials, and planar defects such as crystallographic shear planes [16–20]. Fig. 14 shows the phase diagram of the Ti–O system [21]. Note that the Ti–O system is very rich in stable phases with O/Ti = 1.6–2.0 (seven discrete phases of the homologous series Ti_nO_{2n-1}, where $n \geqslant 4$, have been identified), thereby making the TiO_2 crystal easily reduced. The reduction state is reflected by its color change [19]. Generally, the darker the color, the more heavily the crystal is reduced, which, again, is dependent on the experimental conditions such as annealing temperature, annealing time, atmosphere, etc. The reduction seems to be a bulk phenomenon since the color change appeared not only at the crystal surface but also in the crystal bulk, and no distinct color difference was found in the cross-section of the TiO_2 substrates.

The effect of hydrogen on the TiO_2 reduction is of particular interest. Comparing the color changes of the TiO_2 substrates in vacuum, Ar and Ar–3% H_2 (Fig. 2), one sees that the reduction of TiO_2 is significantly enhanced by the presence of H_2 in the atmosphere. It was reported that molecular hydrogen does not strongly interact with the TiO_2 surface at room temperature [22]; however, at elevated temperatures it does reduce the TiO_2 crystal considerably [23–25]. Zhong et al. [24] investigated the local structure of the defects for hydrogen-reduced (in 1 atm of hydrogen at 1073 K for 2 h) and vacuum-reduced (in an ultrahigh vacuum (UHV) at 1273 K for 2 h) TiO_2 (1 1 0) surfaces and found that both vacuum- and hydrogen-annealing treatments reduced the (1 1 0) rutile crystals, which, in contrast to the stoichiometric surface, exhibit a significant degree of inhomogeneity in both electronic and topographic structures. However, the electronic and geometric features of the two samples are distinct. Two reduction mechanisms, i.e., reduction dominated by the diffusion of hydrogen and hydroxyls for the hydrogen-annealed sample and dominated by the diffusion of oxygen anions (O^-) and vacancies for the vacuum-annealed sample were proposed to account for their difference. In a similar study performed by the same group, Wallace et al. [25] measured the titanium concentration profiles in TiO_2

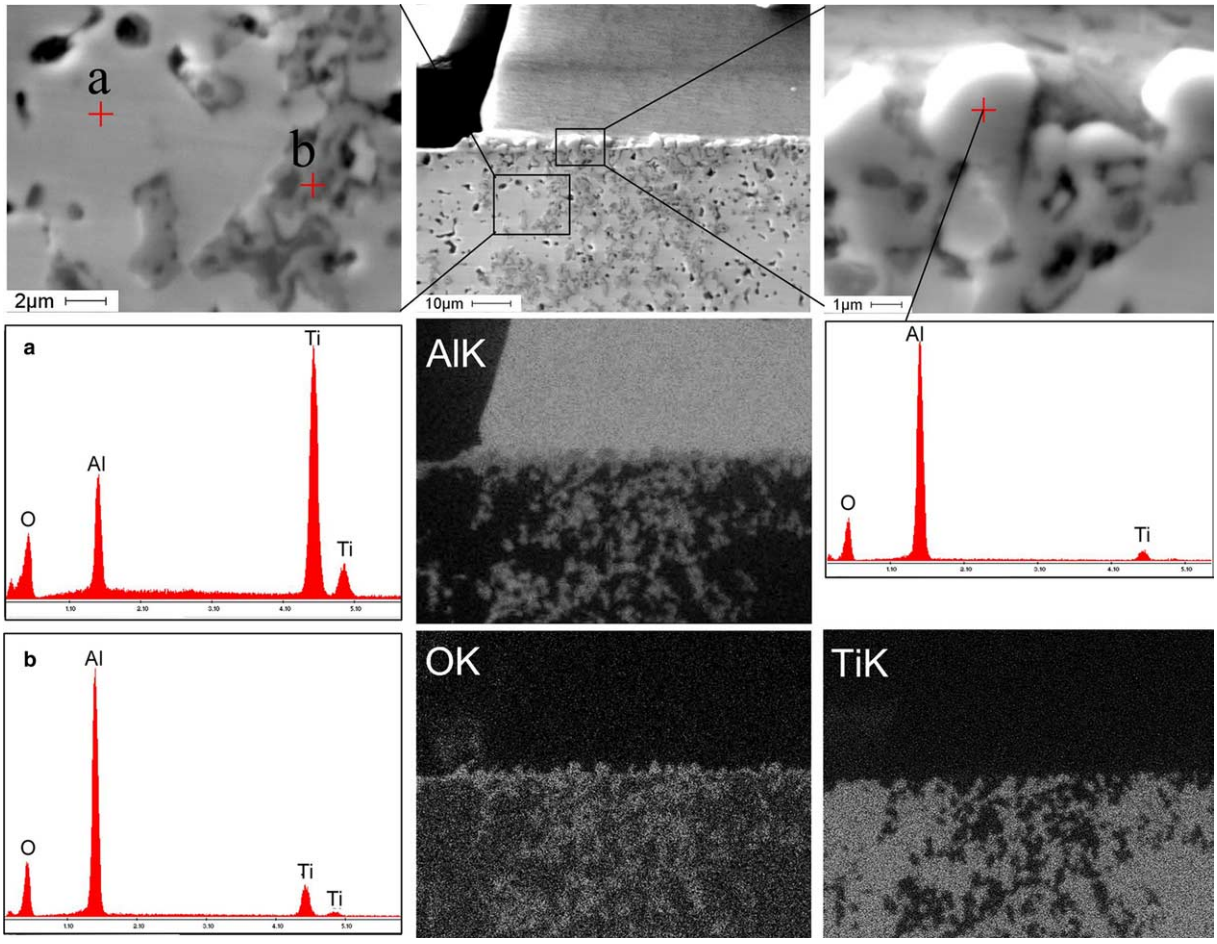

Fig. 11. ESEM micrographs and EDAX results showing the interfacial microstructures and their compositions around the triple junction in the sample tested at 1373 K for 1 h in Ar.

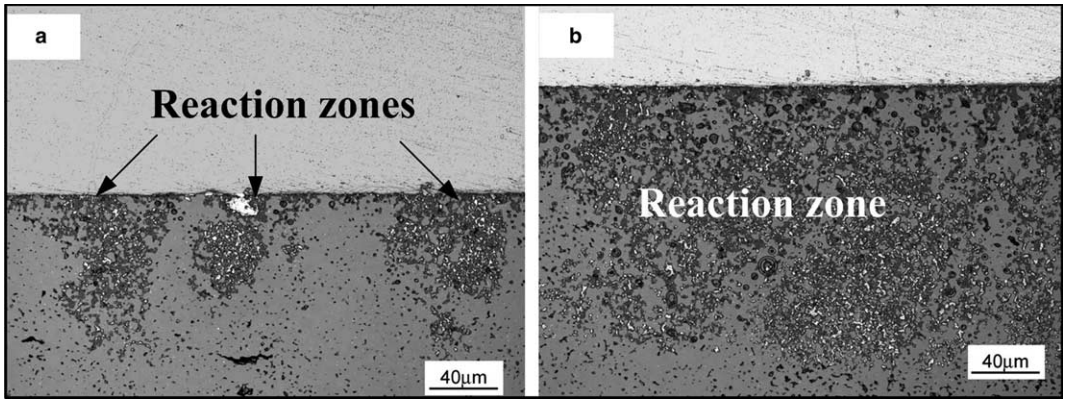

Fig. 12. Laser microscopy images of the interfacial microstructures for the samples tested at 1473 K for 2 h in vacuum for Al dropped (a) without and (b) with mechanical extrusion.

(1 1 0) samples annealed at 973 K in a UHV of 1×10^{-10} torr ($\sim 1.33 \times 10^{-8}$ Pa) for 36 h and at 1073 K in flowing hydrogen for 2 h by means of the Rutherford backscattering spectrometry technique. The surface of the vacuum-annealed sample was estimated to contain about 42% titanium, giving a composition of $TiO_{1.38}$, while that of the hydrogen-annealed sample contained about 38% titanium, yielding a composition of $TiO_{1.63}$. The titanium excess for each sample asymptotically decays to the stoichiometric value at some depth below the surface, suggesting a diffusion-controlled process [25]. In terms of the O/Ti values and the titanium concentration profiles given by them, the degree of the TiO_2 reduction seems to be greater in UHV than in hydrogen. However, the sample treatment

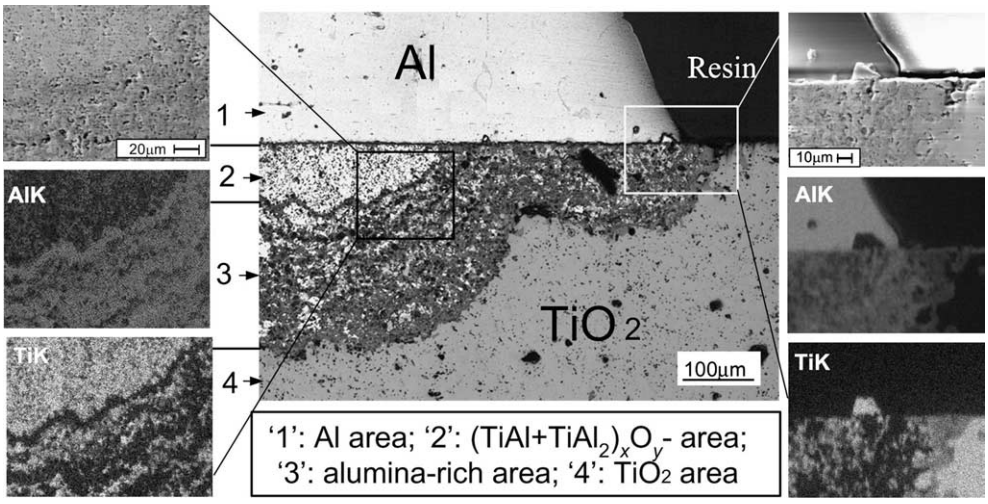

Fig. 13. Microstructures at the interface around the triple junction in the sample tested at 1573 K for 1 h in Ar.

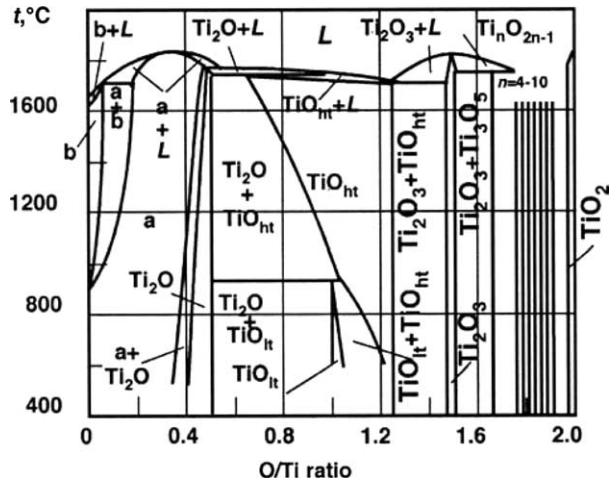

Fig. 14. Phase diagram of the Ti–O system [21]. The Ti_2O_3–TiO_2 region contains Ti_2O_3, Ti_3O_5, seven discrete phases of the homologous series Ti_nO_{2n-1} (Magneli phases) and TiO_2.

conditions (temperature and time) employed in the studies of Wallace et al. are not the same, making it difficult to compare definitively the role of hydrogen playing in TiO_2 reduction with that of vacuum.

Based on the assumption that the reduction in TiO_2 is a diffusion-controlled process, the role of hydrogen might be recognized by considering the oxygen defect creation mechanism and comparing the relevant diffusivity of atomic hydrogen (molecular hydrogen can dissociate at the rutile surface into atomic hydrogen, particularly at sites where a vacancy or step exists [22]) and hydroxyl ions with that of oxygen anions in TiO_2 crystals. As suggested by Zhong et al. [24], the creation of oxygen defects in TiO_2 under vacuum annealing is primarily a thermally activated process and the rate is controlled by the diffusion of the oxygen anion through the lattice towards the surface in response to the oxygen activity gradient. In hydrogen annealing, oxygen defects can be produced by the reaction of hydrogen with lattice oxygen to form hydroxyl ions, which subsequently diffuse outward to the surface and then recombine to form water molecules. Easy entry of hydrogen into the rutile structure and formation of hydroxyl ions were demonstrated by Von Hippel et al. [26] even for the quantities of hydrogen of the order of parts per million of hydrogen to oxygen. The diffusivity of atomic hydrogen in rutile is approximately $3 \times 10^{-6}\,cm^2\,s^{-1}$ at 1073 K, which is about two orders of magnitude higher than that of oxygen [24]. Moreover, the hydroxyl ions, because of their lower negative charge and almost identical ionic radius, should encounter less of an energy barrier than the O^- ions when jumping from an occupied site to a vacancy and would provide a higher diffusivity [27]. Consequently, it appears reasonable that the diffusion of hydrogen into the bulk and the diffusion of hydroxyl ions to the surface are faster than the diffusion of oxygen anions through the lattice towards the surface [24]. In this sense, we postulate that the reduction of TiO_2 is greater in a reducing hydrogen or hydrogen-containing atmosphere than in vacuum and in Ar, yielding a higher oxygen partial pressure around the Al drops, which, in turn, is responsible for the oxidation appearance of the Al drops (Fig. 2). Also, the formation of the alumina smog, as shown in Fig. 6, could be attributed to an extensive reaction between aluminum and water molecules.

Due to the oxygen release from the TiO_2 substrates during annealing, the oxygen partial pressure in the chamber increases, making an accurate measurement of the wettability in the Al–TiO_2 system difficult. Vacuum favors removing oxygen more easily than an atmosphere environment, and therefore the contact angles obtained in vacuum are smaller than those in Ar, which, in turn, are smaller than in Ar–3% H_2. Increasing temperature significantly enhances TiO_2 reduction. Accordingly, the dependence of the initial contact angle on temperature in this system exhibits a distinctive behavior; namely, the initial contact angle is generally larger at a higher

temperature (Figs. 4, 5 and 9). Because of TiO_2 reduction, the wettability measured, from a strict point of view, is no longer for the stoichiometric TiO_2 but for the reduced TiO_2 by molten Al.

4.2. Interfacial reactions and wettability

Thermodynamic consideration of the reactions between Al and TiO_2 as well as its suboxides such as Ti_2O_3 and TiO indicates that they are all energetically favorable [28]. Surface science studies [28–31] show a strong reaction of ultrathin Al films with both stoichiometric and non-stoichiometric (reduced) TiO_2 single crystals at room temperature. For instance, Dake and Lad [28,29] found that Al strongly reduced stoichiometric TiO_2 and sub-stoichiometric TiO_{2-x} surfaces and an aluminum oxide phase was formed at the interface. This aluminum oxide film continued to grow at high Al coverages by extracting oxygen anions from the TiO_2 or TiO_{2-x} bulk when the substrate was annealed in UHV. The Ti species reduced by the Al interaction became re-oxidized during the annealing process and therefore no intermetallic Al–Ti compounds were formed at the interface.

At higher temperatures such as in the wetting experiments, however, the reactions between Al and TiO_2 become more complicated. The overall energetics of the reaction at the Al–TiO_2 interface could be determined by the relative energies of the following competing reactions:

$$\text{Al surface oxidation: } 4Al + 3O_2 \rightarrow 2Al_2O_3 \quad (6)$$

$$\text{Al surface deoxidation: } 4Al + Al_2O_3 \rightarrow 3Al_2O \quad (7)$$

$$\text{Al reaction with } TiO_2 \text{ (actually, the reduced } TiO_2\text{)}: \quad Al + TiO_2 \rightarrow Al_2O_3 + TiO_{2-x} \quad (8)$$

or

$$Al + TiO_2 \rightarrow Al_2O_3 + [Ti]_{Al} \quad (9)$$

Which reaction is dominant depends on the oxygen partial pressure, P_O, around the Al drop as well as the pre-existing oxide film conditions (such as thickness and compactness), which, again, is correlated with temperature, time, atmosphere, testing (dropping) method, etc. The real reaction between Al and TiO_2, in this context, is controlled more by the kinetic factors than by thermodynamic conditions.

There are three kinetic processes that need to be considered: (a) oxygen creation and diffusion in the TiO_2 substrates, (b) Al surface oxidation (Eq. (6)), and (c) Al surface deoxidation (Eq. (7)). Among these, process (a) is the most important, which directly affects processes (b) and (c). If the rates of oxygen creation and diffusion are rapid, the oxygen partial pressure around the Al drop will be sufficiently high to inhibit reactions (7)–(9). This is the case for the samples tested in Ar–3% H_2. In contrast, if the rates of the oxygen creation and diffusion are moderate or even slow, it is possible for process (c) to overwhelm process (b) as long as the kinetic conditions are satisfied. Such a case might be encountered in the Ar and vacuum environments, where oxygen creation and diffusion rates are relatively slower as we have already mentioned.

It should be specifically pointed out that the effect of temperature on the reaction and wetting is a double one. Increasing the temperature considerably enhances TiO_2 reduction since process (a) is primarily thermally dependent. However, process (c) (i.e., reaction (7)) tends to proceed more readily at higher temperatures. Laurent et al. [32] have established a relationship between the equilibrium partial pressure of Al_2O, $P^{eq}_{Al_2O}$, and temperature based on thermodynamic calculations and suggested that, for a fixed oxygen partial pressure, P_O, there is a threshold value of temperature, T_{th}, below which the oxide film thickens and above which it is eroded to deoxidize the surface. Because of the TiO_2 reduction and its induced increase in P_O, it is believed that T_{th} for the Al–TiO_2 system should be higher than that for the Al–Al_2O_3 system under the same experimental conditions. However, it is difficult for us to estimate the value of T_{th} for the Al–TiO_2 system since the TiO_2 reduction kinetics is not well understood. Likewise, the intrinsic wettability between Al and TiO_2 is also difficult to evaluate because the contact angles obtained in the sessile drop experiment are very sensitive to the oxygen partial pressure around the Al drop [14,33]. We can just conjecture that the contact angles obtained in vacuum are closer to the intrinsic ones than those obtained in Ar and Ar–3% H_2, despite the fact that they could still be affected by Al surface oxidation or/and by Al volume loss due to evaporation.

A substantial reaction between Al and TiO_2 (Eq. (9)), as reflected in the interfacial microstructures of the sessile drop samples tested in vacuum and in Ar, seems to proceed only at high temperatures ($T \geqslant 1273$ K). This is different from the behavior observed in the synthesis (such as pressure-aided reactive infiltration and squeeze casting) processes mentioned in Section 1, in which a strong reaction was generally observed at $T \geqslant 1073$ K and alumina-reinforced Ti–Al intermetallic compounds, mainly $TiAl_3$, were formed at the interface [2–6]. It should be pointed out that the experimental conditions in these two cases are quite different. In the sessile drop experiment, disruption of the Al surface oxide film relies primarily on reaction (9), which needs a well-controlled value of P_O as well as a high temperature. In the synthesis processes, the oxide film could be disrupted by some external forces, and consequently an intimate contact of Al with TiO_2 is made more readily, leading to an immediate reaction. The reaction products depend on the Al/TiO_2 ratios, as indicated in the TiO_2–Al pseudobinary phase diagram (see Fig. 15). When liquid Al is predominant, M_2O_3 (M represents either Al or Ti, which may substitute for each other on the $(Al,Ti)_2O_3$ lattice [6]) reinforced $TiAl_3$ or ($Ti_3Al + Al$) composites will be produced. When Al and TiO_2 are equivalent, M_2O_3-reinforced ($TiAl + TiAl_2$) or ($TiAl_2 + TiAl_3$) composites will be obtained.

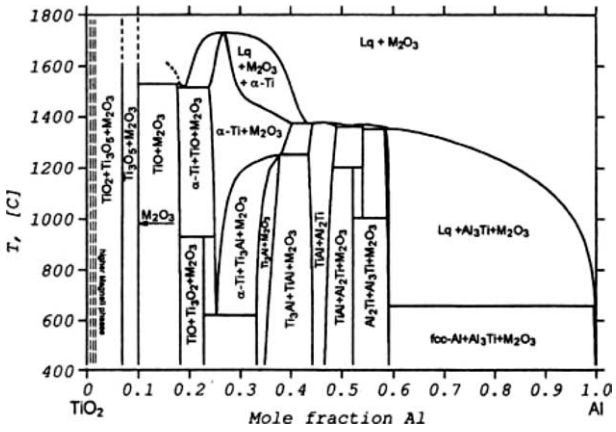

Fig. 15. Calculated TiO_2–Al pseudobinary phase diagram [6].

5. Conclusions

The wettability of polycrystalline rutile TiO_2 by molten Al and factors influencing it such as atmosphere, temperature, time and testing method were thoroughly investigated in this study. With the mechanical disruption of the oxide film, the wettability is substantially improved. The influence of atmosphere is significant. The contact angles measured in vacuum are smaller than those obtained in Ar, which, in turn, are smaller than in Ar–3% H_2. The influence of temperature, however, is not very marked, although the initial contact angles show a distinctive temperature-dependent behavior; they are larger at higher temperatures. With regard to the contact angles obtained in vacuum and in Ar, which are generally smaller than 90°, Al–TiO_2 system is of a partial wetting nature. However, this system can easily be non-wetting due to a considerable increase in oxygen partial pressure around the Al drop as a result of TiO_2 reduction.

Bulk reduction in the TiO_2 crystals during high-temperature annealing was manifested by their distinct color changes. The different colors represent different degrees of reduction. The reduction is both temperature- and atmosphere-dependent. A higher temperature and the presence of hydrogen in the atmosphere significantly enhance the reduction of the crystals. Since the wettability and the reaction as well as the microstructures at the interface regions are mostly dominated by the oxygen partial pressure around the Al drop, they can be directly influenced by the degree of TiO_2 reduction, or, more definitely, by the kinetics of the oxygen creation and diffusion in the TiO_2 crystals. The wetting and reaction results, therefore, could be interpreted in terms of TiO_2 surface reduction kinetics and Al surface oxidation/deoxidation kinetics.

Acknowledgements

This work was supported by the 21st Century COE (Center of Excellence) Program (project: Center of Excellence for Advanced Structural and Functional Materials Design) from the Ministry of Education, Sports, Culture, Science and Technology of Japan.

References

[1] Gaus SP, Harmer MP, Chan HM, Caram HS, Bruhn J, Clauss N. J Am Ceram Soc 2000;83:1606.
[2] Wagner F, Garcia DE, Krupp A, Claussen N. J Eur Ceram Soc 1999;19:2449.
[3] Tsuchitori I, Fukunaga H. J Japan Inst Metals 1992;56:333.
[4] Pan J, Yang DM, Li JH, Ning XG, Ye HQ, Fukunaga H, et al. Compos Sci Technol 1997;57:319.
[5] Beyer P, Janssen R, Claussen N. Adv Eng Mater 2000;2:733.
[6] Gheorghe I, Rack HJ. Metall Mater Trans A 2002;33:2155.
[7] Gheorghe I, Rack HJ. Mater Sci Technol 2002;18:1079.
[8] Claussen N, Garcia DE, Janssen R. J Mater Res 1996;11:2884.
[9] Ying DY, Zhang DL, Newby M. Metall Mater Trans A 2004;35:2115.
[10] Zhang DL, Ying DY, Munroe P. J Mater Res 2005;20:307.
[11] Mortensen A, Jin J. Int Mater Rev 1992;37:101.
[12] Sobczak N, Stobierski L, Radziwill W, Ksiazek M, Warmuzek M. Surf Interf Anal 2004;36:1067.
[13] Avraham S, Kaplan WD. J Mater Sci 2005;40:1093.
[14] Shen P, Fujii H, Matsumoto T, Nogi K. J Am Ceram Soc 2004;87:2151.
[15] Eustathopoulos N, Nicholas MG, Drevet B. Wettability at high temperatures. Oxford, UK: Pergamon/Elsevier Science; 1999.
[16] Bennett RA, Poulston S, Stone P, Bowker M. Phys Rev B 1999;59:10341.
[17] Nörenberg H, Dinelli F, Briggs GAD. Surf Sci 2000;446:L83.
[18] Nörenberg H, Tanner RE, Schierbaum KD, Fischer S, Briggs GAD. Surf Sci 1998;396:52.
[19] Li M, Hebenstreit W, Diebold U, Tyryshkin AM, Bowman MK, Dunham GG, et al. J Phys Chem B 2000;104:4944.
[20] Diebold U, Li M, Dulub O, Hebenstreit ELD, Hebenstreit W. Surf Rev Lett 2000;7:613.
[21] Samsonov GV. The oxide handbook. New York, NY: IFI/Plenum; 1982.
[22] Henrich VE, Kurtz RL. Phys Rev B 1981;23:6280.
[23] Lazarus MS, Sham TK. Chem Phys Lett 1982;92:670.
[24] Zhong Q, Vohs JM, Bonnell DA. J Am Ceram Soc 1993;76:1137.
[25] Wallace WE, Zhong Q, Genzer J, Composto RJ, Bonnell DA. J Mater Res 1993;8:1629.
[26] Hippel AV, Kalnajs J, Westphal WB. J Phys Chem Solids 1962;23:779.
[27] Shannon RD. J Appl Phys 1964;35:3414.
[28] Dake LS, Lad RJ. Surf Sci 1993;289:297.
[29] Dake LS, Lad RJ. J Vac Sci Technol A 1995;13:122.
[30] Lai X, Xu C, Goodman DW. J Vac Sci Technol A 1998;16:2562.
[31] Carroll DL, Liang Y, Bonnell DA. J Vac Sci Technol A 1994;12:2298.
[32] Laurent V, Chatain D, Chatillon C, Eustathopolous N. Acta Metall 1988;36:1797.
[33] John H, Hausner H. J Mater Sci Lett 1986;5:549.